PNAS RESEARCH ARTICLE | CELL BIOLOGY

The CRL3^{gigaxonin} ubiquitin ligase–USP15 pathway governs the destruction of neurofilament proteins

Hyoung-Min Park[a], Ly Le[b], Thao T. Nguyen[c], Ki Hong Nam[d], Alban Ordureau[d], J. Eugene Lee[a], and Thang Van Nguyen[e,1]

Edited by Vishva Dixit, Genentech, San Francisco, CA; received April 19, 2023; accepted September 20, 2023 by Editorial Board Member James A. Wells

Giant axonal neuropathy (GAN) is caused by mutations in the *GAN* gene encoding for gigaxonin (GIG), which functions as an adaptor of the CUL3-RBX1-GIG (CRL3^{GIG}) E3 ubiquitin ligase complex. The pathological hallmark of GAN is characterized by the accumulation of densely packed neurofilaments (NFs) in the axons. However, there are fundamental knowledge gaps in our understanding of the molecular mechanisms by which the ubiquitin–proteasome system controls the homeostasis of NF proteins. Recently, the deubiquitylating enzyme USP15 was reported to play a crucial role in regulating ubiquitylation and proteasomal degradation of CRL4^{CRBN} substrate proteins. Here, we report that the CRL3^{GIG}–USP15 pathway governs the destruction of NF proteins NEFL and INA. We identified a specific degron called NEFL^{L12} degron for CRL3^{GIG}. Notably, mutations in the C-terminal Kelch domain of GIG, represented by L309R, R545C, and C570Y, disrupted the binding of GIG to NEFL and INA, leading to the accumulation of these NF proteins. This accounts for the loss-of-function mutations in GAN patients. In addition to regulating NFs, CRL3^{GIG} also controls actin filaments by directly targeting actin-filament-binding regulatory proteins TPM1, TPM2, TAGLN, and CNN2 for proteasomal degradation. Thus, our findings broadly impact the field by providing fundamental mechanistic insights into regulating extremely long-lived NF proteins NEFL and INA by the CRL3^{GIG}–USP15 pathway and offering previously unexplored therapeutic opportunities to treat GAN patients and other neurodegenerative diseases by explicitly targeting downstream substrates of CRL3^{GIG}.

Gigaxonin | USP15 | neurofilament | GAN

Significance

Giant axonal neuropathy (GAN) is caused by mutations in the *GAN* gene encoding for Gigaxonin (GIG), an adaptor of the CUL3-RBX1-GIG (CRL3^{GIG}) E3 ubiquitin ligase complex. GAN's pathological hallmark is characterized by the accumulation of neurofilaments (NFs) in the axons. However, it has yet to be explored how CRL3^{GIG} regulates the homeostasis of NFs. Here, we find that the CRL3^{GIG}–USP15 pathway governs the destruction of NF proteins NEFL and INA. Furthermore, CRL3^{GIG} controls actin filaments by targeting TPM1, TPM2, TAGLN, and CNN2 for proteasomal degradation. Strikingly, mutations in the Kelch domain of GIG disrupted its binding to NEFL and INA, leading to the accumulation of NF proteins in *GAN*-knockout cells. This accounts for the loss-of-function mutations in GAN patients.

The ubiquitin–proteasome system (UPS) plays a crucial role in almost all critical cellular pathways, and its dysregulation leads to deadly human diseases, including cancer and neurodegenerative diseases (1, 2). Ubiquitylation of protein substrates is catalyzed by the ubiquitin-specific E1, E2, and more than 600 E3 ligases, and can be reversed by ~100 deubiquitylating enzymes (DUBs) (3). The cullin-RING ubiquitin ligases (CRLs) represent a major family of multicomponent RING-class E3 complexes, composed of four subunits: a cullin scaffold, an E2-recruiting RING domain protein (RBX1 or RBX2), an adaptor, and a substrate receptor (4, 5). In mammals, there are eight human cullins (CUL1, CUL2, CUL3, CUL4A, CUL4B, CUL5, CUL7, and CUL9) (6). For example, CUL3 interacts with BTB domain proteins, encoded by approximately 180 genes in the human genome (7), which function as both substrate adaptors and receptors in a single protein (8–11). The BTB domains can also facilitate self-assembly to form dimers, leading to the formation of CUL3-Adaptor^{BTB} E3 homodimers (12–14). However, little is known about how CRL3 E3 ligases control ubiquitylation and proteasomal degradation of downstream substrates under neurodegenerative disorders.

In eukaryotes, the cytoskeleton comprises three types of filaments: microtubules, microfilaments (known as actin filaments), and intermediate filaments (IFs). IF proteins, encoded by 73 genes, are classified into six types (I–VI), based on sequence homology (15). The type I and type II groups are the acidic and basic keratins, respectively. The type III group includes vimentin (VIM), desmin (DES), glial fibrillary acidic protein (GFAP), and peripherin (PRPH), while the nuclear lamins are categorized as type V. Tanabin, transitin, and nestin are type VI (16). Neurofilaments (NFs), classified as type IV IF proteins, are composed of 4 subunits: NF heavy (200 kDa), medium (145–160 kDa), and light polypeptide (68–70 kDa) (NFH, NFM, and NFL, respectively; hereafter referred to as NEFH, NEFM, and NEFL), and a-internexin (INA, 59–65 kDa) in mature neurons in the central nervous system (CNS) (17, 18). In neurons in the peripheral nervous system (PNS), NFs include NEFH, NEFM, NEFL, and PRPH (57–58 kDa) (18). Despite recent advances in understanding neurofilament biology and pathophysiology, numerous fundamental questions remain unanswered. Specifically, how does the UPS regulate the turnover of NF subunits identified as extremely "long-lived" proteins? Which DUBs and E3 ubiquitin ligases are involved in maintaining the homeostasis of

Author contributions: H.-M.P., L.L., A.O., J.E.L., and T.V.N. designed research; H.-M.P., L.L., T.T.N., K.H.N., and T.V.N. performed research; T.V.N. contributed new reagents/analytic tools; H.-M.P., L.L., T.T.N., K.H.N., A.O., J.E.L., and T.V.N. analyzed data; T.V.N. conceived the study and supervised research; and T.V.N. wrote the paper.

The authors declare no competing interest.

This article is a PNAS Direct Submission. V.D. is a guest editor invited by the Editorial Board.

[1]To whom correspondence may be addressed. Email: nguyentv@health.missouri.edu.

This article contains supporting information online at https://www.pnas.org/lookup/suppl/doi:10.1073/pnas.2306395120/-/DCSupplemental.

Published October 30, 2023.

NFs? What is the significance of NF turnover in contributing to neurodegenerative diseases?

Giant axonal neuropathy (GAN), first described in 1972 by Berg and colleagues, is a rare hereditary autosomal recessive neurodegenerative disorder (19, 20). The pathological hallmark of GAN is characterized by the accumulation of densely packed NFs in the axons of PNS and CNS (21, 22). GAN patients manifest severe early-onset motor and sensory axonal neuropathy with CNS involvement and characteristic "kinky" hair around 3–5 y of age. Their death usually occurs in the second to third decade of life (23). In 2000, Bomont and colleagues identified the disease-causing gene *GAN* encoding Gigaxonin protein (GIG) (24). GIG comprises an amino-terminal BTB domain and a C-terminal Kelch domain (24). Based on sequence homology (7) and the structural study of CUL3-GIG^{BTB} homodimer complex (12), GIG (also known as KLHL16) may function as an adaptor in the CUL3-RBX1-GIG (known as CRL3^{GIG}) E3 ubiquitin ligase complex and regulate diverse substrates. However, it is not known whether CRL3^{GIG} could ubiquitylate specific substrates in vitro and in vivo. What is a specific degradation signal on substrates (degron) that binds GIG, leading to ubiquitylation and degradation of CRL3^{GIG} substrates? What are the mechanisms of pathogenesis in patients carrying *GAN* mutations?

Targeted protein degradation by the UPS is an important therapeutic modality in drug discovery to target previously undruggable disease-causing proteins for destruction (25–27). The molecular glue and PROTAC degraders hijack E3 ubiquitin ligases, leading to ubiquitylation and subsequent degradation of protein targets. A recent study by Nguyen has reported that USP15 antagonizes CRL4^{CRBN}-mediated ubiquitylation of glutamine synthetase (GS) and neosubstrates, thereby preventing their degradation (28). Targeting USP15 sensitizes the immunomodulatory drug (IMiD)-sensitive and resistant multiple myeloma cells to lenalidomide by promoting the degradation of neosubstrates. USP15 diminishes the action of molecular glue Cereblon E3 ligase modulator (CELMoD) and CRBN-based PROTAC degraders by antagonizing the activity of the CRL4^{CRBN} (28). However, whether USP15 may regulate the downstream substrates of other CRL E3 ligases is largely unknown.

In the present study, we addressed multiple "long-standing" questions. We found that the CRL3^{GIG}-USP15 pathway is required to regulate long-lived NF proteins NEFL and INA. In addition to regulating NFs, CRL3^{GIG} also controls another class of cytoskeleton proteins by targeting the destruction of actin filament–binding regulatory proteins such as TPM1, TPM2, TAGLN, and CNN2. We further identified a specific degron called NEFL^{L12} degron for CRL3^{GIG}. This fundamental knowledge is essential because it helps us further understand the molecular basis of GAN pathogenesis and opens previously unexplored opportunities for developing novel targeted therapies to treat neurodegenerative diseases.

Results

USP15 Controls the Stability of NF Proteins. To systemically characterize the alteration of proteome profile in wild-type (WT) versus *USP15*-knockout (KO) 293FT cells (28), and to search for potential USP15 substrates, we performed the proteome profiling analyses of WT and *USP15*-KO 293FT cells and quantified 8,757 proteins (Fig. 1*A*, *SI Appendix*, Fig. S1, and Dataset S1). A total of 22 proteins were significantly down-regulated (Fig. 1*A* and *SI Appendix*, Table S1*A*), while 20 proteins were up-regulated in *USP15*-KO 293FT cells (Fig. 1*A* and *SI Appendix*, Table S1*B*). GS, a well-characterized substrate of USP15, was down-regulated in *USP15*-KO 293FT cells (*SI Appendix*, Table S1*A*) (28). Notably, the top 10 most down-regulated proteins included two NF proteins NEFL and INA (Fig. 1*A* and *SI Appendix*, Table S1*A*). NF proteins are mainly expressed in neurons and present predominantly in axons, which play a crucial role in maintaining axon caliber and the transmission of electrical impulses along axons (17). Previous studies indicated that HEK293 (or derivative) cells express all 4 NF subunits (29), and they are widely used to study NFs such as translational regulation of *NEFM* and *NEFL* mRNAs by the UBR1/UBR2-mediated Arg/N-degron pathway (30) or the GIG-IF interaction network (31). Therefore, 293FT cell lines were chosen for our biochemical studies.

To validate our proteomic data, we treated WT and *USP15*-KO 293FT cells with the NEDD8-activating enzyme inhibitor MLN4924, which inactivates CRL activity (32) and analyzed by Western blot. Consistent with the proteomic data (Fig. 1*A*), the steady-state levels of NEFL and INA were significantly down-regulated in *USP15*-KO 293FT cells (Fig. 1 *B* and *C*). MLN4924-treated cells stabilized at least twofold the protein level of NEFL, and to a lesser extent INA protein level in *USP15*-KO 293FT cells, which was similar to the results observed in GS protein level (28) (Fig. 1*B*). Depletion of USP15 by short hairpin RNA (shRNA) knockdown (KDO) down-regulated NEFL and INA protein levels in the neuroblastoma cell line SH-SY5Y (*SI Appendix*, Fig. S2*A*). Depletion of USP15, but not other DUBs, including USP7 and USP11, caused the downregulation of NEFL, INA, and GS proteins (Fig. 1*B* and *SI Appendix*, Fig. S2 *A* and *C*). These findings suggest that USP15 might play an essential role in regulating the stability of NF proteins.

NF proteins exhibit exceptionally long half-lives (17); however, our cycloheximide (CHX) chase experiments revealed that both NEFL and INA were significantly degraded in *USP15*-KO 293FT cells (Fig. 1 *D* and *E*). The downregulation and the enhanced degradation rate of endogenous NEFL, INA, and GS proteins in *USP15*-KO 293FT cells were blunted by overexpressing WT USP15^{Flag}, but not empty vector or a catalytically inactive C298A-USP15^{Flag} mutant (Fig. 1 *F* and *G* and *SI Appendix*, Fig. S2 *D* and *E*). Our RNA-sequencing (RNA-seq) analysis showed that the mRNA levels of *NEFL* and *INA* were unchanged in *USP15*-KO 293FT cells and MLN4924-treated *USP15*-KO 293FT cells (*SI Appendix*, Figs. S3 and S4 and Datasets S2 and S3). These data indicated that the molecular control of USP15-mediated degradation of NEFL and INA was a posttranslational mechanism and that USP15 may control their ubiquitylation status and subsequent degradation by the proteasome. To test this idea, we performed TUBE2 pulldown experiments in cells treated with the proteasome inhibitor bortezomib (Bort) (33). We found that the ubiquitylated forms of NEFL were significantly accumulated in Bort-treated *USP15*-KO 293FT cells (Fig. 1*H*). In line with the results observed in 293FT cell lines (Fig. 1*H*), *USP15*-depleted SH-SY5Y cells increased ubiquitylated forms of NEFL and INA (*SI Appendix*, Fig. S2*B*). Overexpression of WT USP15^{Flag} completely abrogated polyubiquitylated NEFL, while a C298A-USP15^{Flag} mutant failed to deubiquitylate polyubiquitylated NEFL in *USP15*-KO 293FT cells (Fig. 1*I*). Strikingly, recombinant USP15 enzyme (rUSP15) purified from insect cells efficiently deubiquitylated polyubiquitylated NEFL in vitro (Fig. 1*J*). Collectively, our data strongly indicated that USP15 plays an important role in regulating the stability of NEFL and INA in a CRL E3 ubiquitin ligase-dependent fashion.

Depletion of GAN Resulted in the Accumulation of NF Proteins and Actin Filament–Associated Regulatory Proteins. Since we uncovered a pathway in the UPS, including USP15, proteasome, and a putative CRL ubiquitin ligase to control the stability of NEFL and INA, we next sought to identify the CRL E3

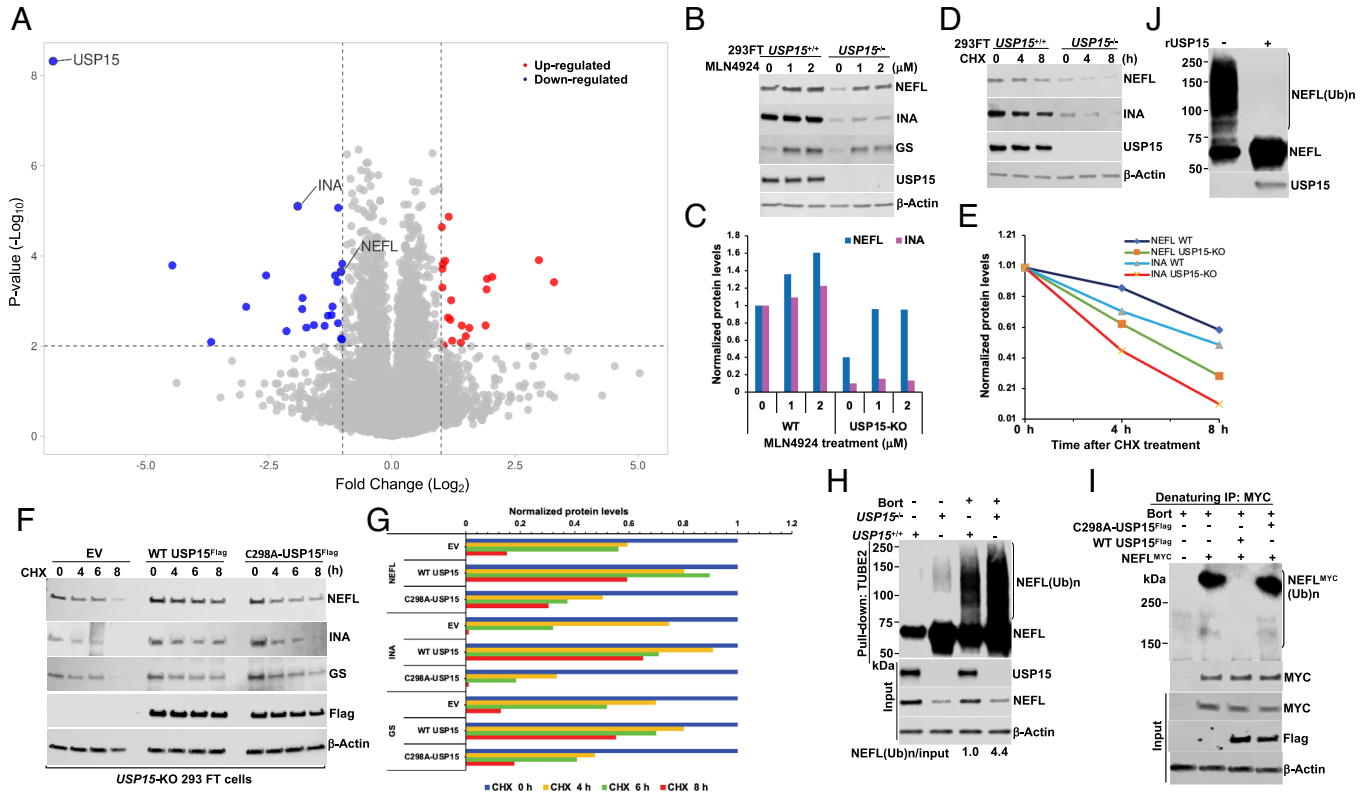

Fig. 1. USP15 controls the stability of NF proteins. (*A*) Global proteome analysis of WT and *USP15*-KO 293FT cells. The threshold of fold changes was set to more than a twofold increase or decrease, and the $-\text{Log}_{10}$ *P*-value was above 2; two biological and technical replicate samples were subject to mass spectrometric analysis. (*B*) Validation of proteomic data. WT and *USP15*-KO 293FT cells were treated with different concentrations of MLN4924 (0, 1, and 2 μM) for 8 h. Cell extracts were analyzed by immunoblotting (IB) with the indicated antibodies. (*C*) Quantification of NEFL and INA proteins from (*B*). (*D*) CHX experiment. $USP15^{+/+}$ and $USP15^{-/-}$ 293FT cells were treated with cycloheximide (CHX, 50 μg/mL) at the indicated times. Cell extracts were analyzed by IB. (*E*) Quantification of NEFL and INA proteins from (*D*). (*F*) *USP15*-KO 293FT cells were transiently transfected with empty vector (EV, control), WT $\text{USP15}^{\text{Flag}}$, or $\text{C298A-USP15}^{\text{Flag}}$ mutant plasmid. After 40 h, cells were treated with CHX for the indicated times. Cell extracts were analyzed by IB with the indicated antibodies. (*G*) Quantification of NEFL, INA, and GS proteins from (*F*). The relative ratios of indicated proteins:Actin, normalized to time 0, are shown. (*H*) $USP15^{+/+}$ and $USP15^{-/-}$ 293FT cells were treated with bortezomib (Bort, 1 μM) for 7 h. Total ubiquitylated proteins were purified using TUBE2-agarose. Bound fractions and input were analyzed by IB. (*I*) *USP15*-KO 293FT cells were transiently transfected with NEFL^{MYC} in the presence of EV, WT $\text{USP15}^{\text{Flag}}$, or $\text{C298A-USP15}^{\text{Flag}}$ mutant plasmid. After 40 h, cells were treated with 2 μM bortezomib for 6 h, followed by cell lysis and MYC IP under denaturing conditions. The bound fractions and input were analyzed by IB with antibodies against ubiquitin (*Top*), MYC, Flag, and Actin. (*J*) In vitro deubiquitylation assay. $USP15^{-/-}$ 293FT cells were treated with 1 μM Bort for 7 h. Total ubiquitylated proteins, purified using TUBE2, were treated with recombinant (r)USP15 and then analyzed by IB with anti-NEFL and anti-USP15 antibodies. (Ub)n, polyubiquitin. The results shown are representative of three independent experiments (*B*, *D*, *F*, and *H–J*).

ligase involved in this process. Consistent with our results that MLN4924 suppressed the degradation of NEFL and INA in *USP15*-KO 293FT cells (Fig. 1*B*), a previous study by Emanuele and colleagues focused on the global identification of modular Cullin-RING ligase substrates revealed NEFL protein as one of the top candidates in the CRL3 and MLN4924 GPS screens (34). GIG was particularly interesting among all potential CUL3 adaptors because NF proteins were markedly accumulated in GAN patients (19). Notably, the crystal structure of the GIG^{BTB} domain confirmed that GIG is a CUL3 adaptor (12). Based on these previous studies and our results (Fig. 1*B*), we hypothesized that CRL3^{GIG} controls the turnover of NEFL and other potential substrates. We first generated *GAN*-KO 293FT cells by CRISPR/Cas9 gene editing to test this hypothesis and found that 15 of 26 clones were completely knockout (*SI Appendix*, Fig. S5). Interestingly, all *GAN*-KO 293FT cells accumulated NEFL protein levels (*SI Appendix*, Fig. S5).

To broadly understand how the proteome is remodeled and to search for potential GIG substrates, we performed multiplexed quantitative proteomics on total-cell extracts of WT and two *GAN*-KO 293FT cell lines (*GAN*-KO2 and *GAN*-KO16) and quantified 8,124 proteins (Fig. 2*A*, *SI Appendix*, Fig. S6, and Dataset S4). NF proteins NEFL and INA, along with actin filament–associated regulatory proteins TPM1, TPM2, and TAGLN, were significantly up-regulated in both *GAN*-KO2 and *GAN*-KO16 293FT cell lines (Fig. 2*A*). BRMS1 and CCN2 protein levels were also up-regulated (Fig. 2*A*). We perform RNA-seq analysis and found that the mRNA levels of *NEFL*, *INA*, *TPM1*, *TPM2*, and *TAGLN* remained unchanged in *GAN*-KO 293FT cells, suggesting that their upregulation in protein levels was a posttranslational regulation. In contrast, the mRNA level of CCN2 was significantly up-regulated (*SI Appendix*, Fig. S7 and Dataset S5), suggesting that its increased protein level, observed in proteomic data (Fig. 2*A*), was due to altered transcription.

To validate our proteomic data, we performed western blot using cell extracts from WT, *GAN*-KO2, and *GAN*-KO16 293FT cell lines and found that the steady-state protein levels of NEFL, INA, TPM1, and TAGLN were significantly up-regulated in two *GAN*-KO 293FT cell lines, whereas those of TPM2 and BRMS1 were slightly increased (Fig. 2 *B* and *C*). Although not listed as the most up-regulated protein, CNN2, another actin filament–binding regulatory protein, was elevated in two *GAN*-KO 293FT cell lines based on our Western blot analysis (Fig. 2 *B* and *C*). Furthermore, we adopted the SH-SY5Y cell line as a neuronal cell model to validate our findings. Consistent with the results obtained in *GAN*-KO 293FT cells, knock-down of *GAN* in SH-SY5Y cells by two independent GIPZ shRNAs up-regulated NEFL, INA, TPM1, TAGLN, and CNN2 protein levels (Fig. 2 *D* and *E* and *SI Appendix*,

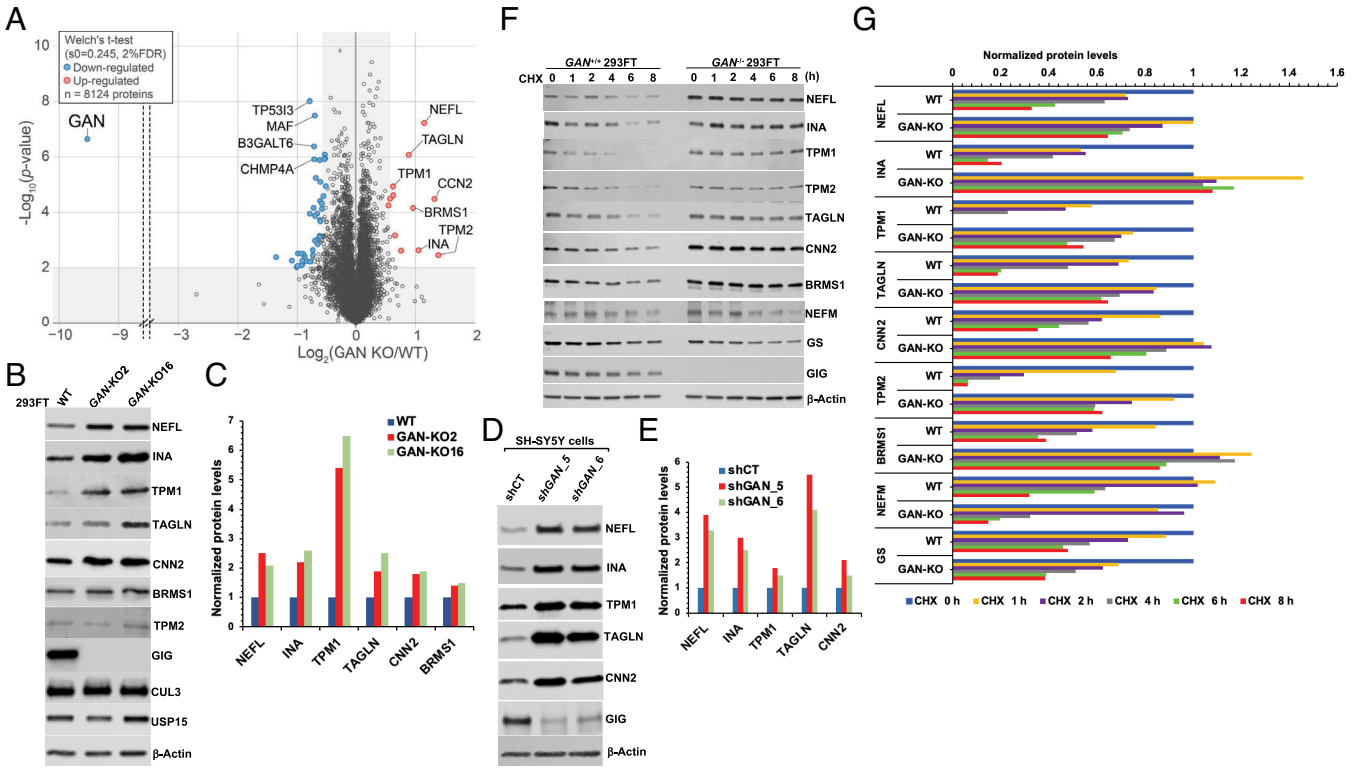

Fig. 2. Depletion of GAN resulted in the accumulation of NF proteins and actin filament–associated regulatory proteins. (*A*) Comparative proteome analysis of WT (*n* = 4), *GAN*-KO2 (*n* = 3), and *GAN*-KO16 (*n* = 3) 293FT cell lines from 10plex TMT analysis. The data are depicted as a volcano plot where both GAN KO clones were combined (*n* = 6). The red and blue dots denote statistically significant enriched or reduced proteins, respectively. (*B*) Validation of proteomic data. Cell extracts from WT, *GAN*-KO2, and *GAN*-KO16 293FT cell lines were analyzed by IB with the indicated antibodies. (*C*) Quantification of NEFL, INA, TPM1, TAGLN, CNN2, and BRMS1 proteins from (*B*). (*D*) Cell extracts from SH-SY5Y cells, stably expressing shRNA control (shCT) and shRNAs targeting GAN clones 5 and 6 (shGAN_5, shGAN_6), were analyzed by IB with the indicated antibodies. (*E*) Quantification of NEFL, INA, TPM1, TAGLN, and CNN2 proteins from (*D*). (*F*) CHX experiment. WT and *GAN*-KO2 293FT cells were treated with CHX for the indicated times. Cell extracts were analyzed by IB. (*G*) Quantification of NEFL, INA, TPM1, TAGLN, CNN2, TPM2, BRMS1, NEFM, and GS proteins from (*F*). The relative ratios of indicated proteins:Actin, normalized to time 0, are shown. The results shown are representative of at least three independent experiments (*B*, *D*, and *F*).

Fig. S8 *A* and *B*). Remarkably, our CHX experiments indicated that the degradation of NEFL, INA, TPM1, TPM2, TAGLN, CNN2, and BRMS1 was blunted in *GAN*-KO 293FT cells and *GAN*-KDO SH-SY5Y cells (Fig. 2 *F* and *G* and *SI Appendix*, Fig. S8 *C* and *D*), further confirming that the turnover of these proteins was dependent on GIG. $CRL4^{CRBN}$-dependent GS degradation was unaffected (Fig. 2 *F* and *G*), indicating that the UPS was intact in *GAN*-KO 293FT cells. Consistent with the proteomic analysis of *GAN*-KO 293FT cell lines (Dataset S4), we also found in our CHX experiments that GIG was not required for the turnover of NEFM (Fig. 2 *F* and *G*), suggesting that targeting NF proteins for the $CRL3^{GIG}$-mediated degradation was selective to NEFL and INA.

Earlier studies on GAN pathology revealed the accumulation of NFs in neurons and did not distinguish which NF proteins were affected (19, 20). In 1983, Ionasescu and colleagues studying NF proteins from neurons of GAN patients reported that the amount of 68,000-Da neurofilament protein (corresponding to NEFL) was two times higher in the GAN nerve than in the control nerve, while the amounts of other NF subunits with 160,000 and 210,000 Da (corresponding to NEFM and NEFH, respectively) were normal (35). This work suggested that GIG mutants in GAN patients, which caused a loss of function, could not ubiquitylate NEFL, leading to the accumulation of NEFL in neurons, whereas GIG did not regulate NEFM and NEFH. Subsequent studies by Johnson-Kerner and colleagues reported that NEFL, and to a lesser extent PRPH, but not NEFM, NEFH, and VIM, were up-regulated in induced pluripotent stem cells (iPSCs) from GAN patients (36). Consistent with these previous studies and our results (Fig. 2 *A*–*G*), the NEFL protein levels in the brains of *GAN*-KO mice were markedly increased (37, 38).

We also noted that a small fraction of endogenous NEFL protein levels was degraded in *GAN*-KO 293FT cells (Fig. 2 *F* and *G*), suggesting that other E3s may be involved in the proteasomal degradation of NEFL. In agreement with this possibility, a previous study showed that the E3-ubiquitin ligase TRIM2 regulates NEFL ubiquitylation (39). In GAN patients, aggregates of IFs in multiple tissues suggest that $CRL3^{GIG}$ may control a vast repertoire of substrates. In line with this argument, the *GAN* mRNA expression profile in diverse human tissues revealed that *GAN* mRNA is highly expressed in multiple tissues, including the heart, liver, kidney, skeletal muscle, and brain (*SI Appendix*, Fig. S9). Taken together, our results demonstrated that $CRL3^{GIG}$ controls the stability of at least two types of substrates, including NF proteins NEFL and INA, and actin filament–associated regulatory proteins TPM1, TPM2, TAGLN, and CNN2.

$CRL3^{GIG}$ Directly Ubiquitylates NF Proteins and Actin Filament–Associated Regulatory Proteins. To explore the molecular mechanisms by which $CRL3^{GIG}$ regulates the stability of NF proteins, we focused on identifying the GIG-NEFL interaction. In line with the previous studies (31, 40), we also found that GIG interacted with NF proteins NEFL and INA in cells overexpressing GIG^{Flag} (Fig. 3 *A* and *B*). Moreover, we performed endogenous IP and confirmed that endogenous NF proteins NEFL and INA interacted with endogenous GIG (Fig. 3*C*). The

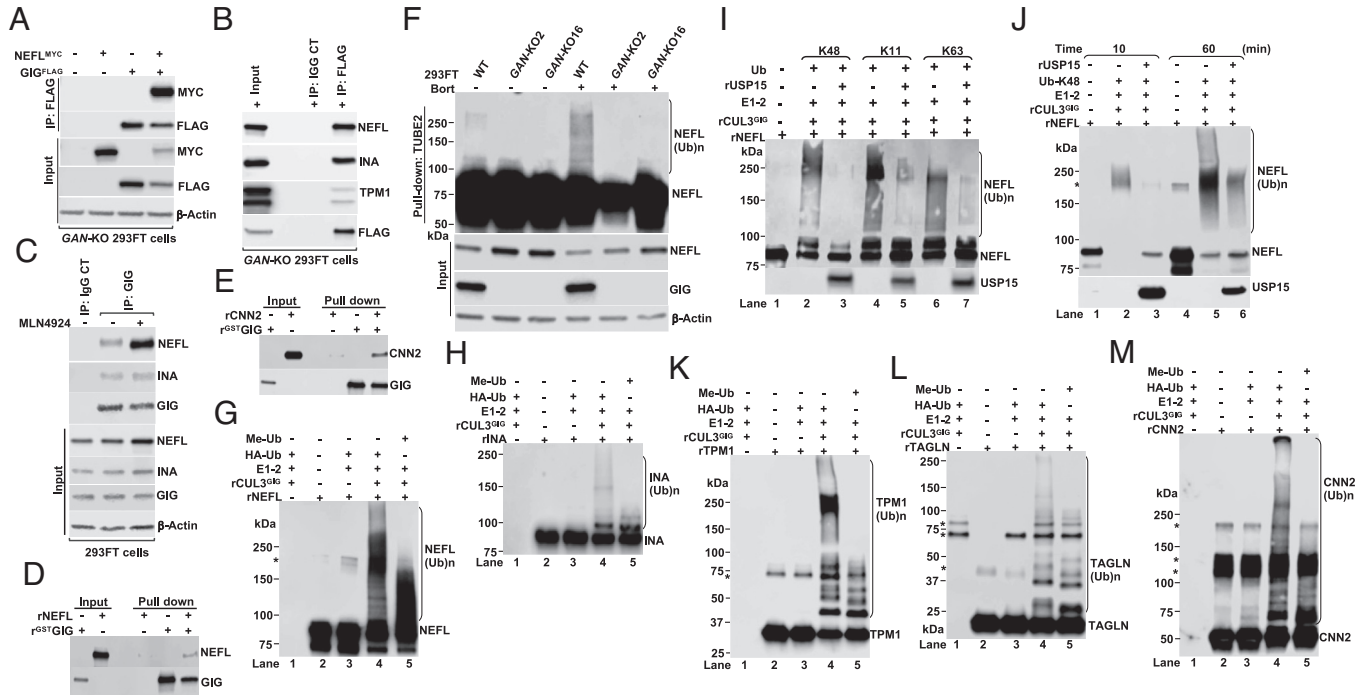

Fig. 3. CRL3^{GIG} directly ubiquitylates NF proteins and actin filament–associated regulatory proteins. (*A*) *GAN*-KO 293FT cells were transfected with the indicated plasmids expressing GIG^{FLAG} and MYC-tagged NEFL (NEFL^{MYC}) for 40 h. Cellular extracts were immunoprecipitated with anti-Flag antibody, followed by IB with antibodies against MYC and FLAG. (*B*) *GAN*-KO 293FT cells were transfected with wild-type GIG^{FLAG}. After 48 h, cell extracts were immunoprecipitated with anti-FLAG or IgG control antibody, followed by IB with the indicated antibodies. (*C*) Endogenous NEFL and INA proteins interact with endogenous GIG. 293FT cells were treated with or without 2 μM MLN4924 for 4 h. Protein extracts were IP with rabbit IgG control or GIG antibody. IP and input samples were analyzed by IB with the indicated antibodies. (*D* and *E*) The direct interactions between GST-GIG and NEFL (*D*) or CNN2 (*E*) in GST pull-down assays. At least two experimental replicates were repeated to optimize conditions (*A*–*E*). (*F*) Cells were treated with or without bortezomib (Bort, 1 μM) for 6 h. Total ubiquitylated proteins were purified using TUBE2-agarose. Bound fractions were analyzed by IB. (*G* and *H*) In vitro ubiquitylation reactions of rNEFL (*G*) and rINA (*H*) were carried out in the presence or absence of E1, E2, HA-tagged ubiquitin (^{HA}Ub) or methylated ubiquitin (Me-Ub), and rCUL3^{GIG} complex. *Indicates a nonspecific band. (*I*) In vitro competitive ubiquitylation and deubiquitylation assay of NEFL was carried out in the presence of rNEFL, E1, E2, rCUL3^{GIG} complex, ubiquitin mutants with K48 only, K11 only or K63 only and rUSP15. (*J*) Same as (*I*), except that reactions were collected at 10 min and 60 min. (*K*–*M*) In vitro ubiquitylation reactions of rTPM1 (*K*), rTAGLN (*L*), and rCNN2 (*M*). The results shown are representative of at least three independent experiments (*F*–*M*).

NEFL/INA-GIG interaction was enhanced in MLN4924-treated 293FT cells (Fig. 3*C*). Notably, the GIG-NEFL interaction was direct since it was confirmed by the in vitro pulldown experiments using recombinant proteins (Fig. 3*D*). We also found that GIG interacted with actin filament–associated regulatory proteins TPM1 and CNN2 in vivo and in vitro (Fig. 3 *B* and *E*), but we did not pursue further in the current work.

To provide direct evidence supporting our central hypothesis that CRL3^{GIG} may ubiquitylate NF proteins NEFL and INA in vitro, we first performed the in vivo ubiquitylation assays using TUBE2 pull-down. As shown in Fig. 3*F*, the polyubiquitylated forms of NEFL, (NEFL(Ub)n) were significantly enriched in WT 293FT cells, which were treated with the proteasome inhibitor bortezomib. In contrast, NEFL(Ub)n were completely absent in two independent *GAN*-KO 293FT cell lines (Fig. 3*F*), suggesting that GIG is required for the ubiquitylation of NEFL in cells. Consistent with these findings, a similar result was observed in *GAN*-KDO SH-SY5Y cells (*SI Appendix*, Fig. S10*A*). USP15-mediated downregulation of NEFL and INA proteins was rescued by MLN4924 treatment in *USP15*-KO 293FT cells (Fig. 1 *B* and *C*) or by *GAN* KDO in *USP15*-KO 293FT cells using three independent GIPZ shRNAs targeting *GAN* (*SI Appendix*, Fig. S10 *B* and *C*), suggesting that USP15 regulates the degradation of NEFL and INA in downstream of CRL3^{GIG}. Remarkably, our in vitro ubiquitylation assays using all recombinant proteins (rUb, rE1, rE2, rCRL3^{GIG}, and rNEFL) strongly demonstrated that rCRL3^{GIG} efficiently ubiquitylated rNEFL (Fig. 3*G*, lane 4, and *SI Appendix*, Fig. S11*A*), and the reaction was inhibited by adding methylated ubiquitin (Me-Ub) (Fig. 3*G*, lane 5 and *SI Appendix*, Fig. S11*A*). In addition, rINA was ubiquitylated by rCRL3^{GIG} in vitro (Fig. 3*H* and *SI Appendix*, Fig. S11*B*). We next asked whether USP15 could deconjugate different polyubiquitin chains of NEFL in vitro. We performed the in vitro competitive ubiquitylation/deubiquitylation assays using all critical components of the UPS: (rUb, rE1, rE2, rCRL3^{GIG}, rNEFL, and rUSP15). As illustrated in Fig. 3 *I* and *J* and *SI Appendix*, Fig. S11 *C* and *D*, USP15 substantially antagonized CRL3^{GIG}-mediated K48-, K11-, or K63-linked polyubiquitylation of NEFL. These results indicated that the CRL3^{GIG}-USP15 pathway directly controls the turnover of NF proteins NEFL and INA.

Although this study was mainly focused on the molecular control of NF degradation by the UPS, we also sought to determine whether CRL3^{GIG} may ubiquitylate actin filament–associated regulatory proteins in vitro. Polyubiquitylation of rTPM1, rTAGLN, and rCNN2 was readily detected by the addition of rCRL3^{GIG}, while it was blocked by the addition of methylated ubiquitin (Fig. 3*K* and *SI Appendix*, Fig. S11*E*; Fig. 3*L* and *SI Appendix*, Fig. S11*F*; and Fig. 3*M* and *SI Appendix*, Fig. S11*G*, respectively). All these actin filament–associated regulatory proteins were also natural substrates of CRL3^{GIG}. Together, CRL3^{GIG} controls both NFs and actin filaments, possibly in neurons and other cell types, respectively.

Mutations in GAN Patients at Amino Acid Residues L^{309}, R^{545}, and C^{570} in the Kelch Domain of GIG Fail to Interact with NF Proteins and Exhibit a Loss-of-Function Mechanism. To further study the functional significance of GIG–NEFL interaction based

on GAN mutations in human patients (24), we first analyzed the sequence alignment of Gigaxonin orthologs across species. We found that mutations in GAN patients at amino acid residues (L^{309}, R^{545}, and C^{570}) in the Kelch domain of GIG were highly conserved across species (Fig. 4*A* and *SI Appendix*, Fig. S12). It was likely that these point mutations may cause detrimental effects on the turnover of NEFL, leading to its accumulation in GAN patients (19, 35). Moreover, GAN is an autosomal recessive genetic disorder, suggesting that the molecular disease mechanism is due to loss-of-function mutations. To investigate this hypothesis, we first performed IP experiments. We found that the binding of L309R, R545C, and C570Y mutants and, to a lesser extent, E486K mutant to endogenous NEFL and INA was significantly disrupted (Fig. 4 *B* and *C*). Next, we sought to test whether the GIG-dependent upregulation of endogenous NEFL protein levels may be rescued by introducing empty vector (EV, control), WT GIG^{FLAG}, L309R, and C570Y mutants in *GAN*-KO 293FT cells and found that only WT GIG^{FLAG} but not EV, L309R, or C570Y mutant greatly down-regulated the endogenous protein levels of NEFL and INA in *GAN*-KO 293FT cells (Fig. 4 *D* and *E*). The molecular phenotype of the C570Y mutant exerted a more robust effect since it completely lost its function in destabilizing endogenous protein levels of NEFL and INA (Fig. 4 *D* and *E*). These findings account for a loss-of-function mechanism in GAN patients.

To systemically characterize the proteome remodeling induced by WT GIG^{FLAG}, L309R, and C570Y mutants in *GAN*-KO 293FT cells, we performed the proteome profiling analysis of *GAN*-KO 293FT cell lines transiently transfected with EV, WT GIG^{FLAG}, L309R, and C570Y mutants. Consistent with western blot analysis (Fig. 4 *D* and *E*), our proteomic data revealed that NEFL and INA protein levels were markedly down-regulated in *GAN*-KO 293FT cells transfected with WT GIG^{FLAG}, while L309R and C570Y mutants failed to destabilize NEFL and INA proteins (Fig. 4 *F–H*, *SI Appendix*, Fig. S13 *A–C*, and Dataset S6). We also found that the protein levels of CUL3 and glutamine synthetase (GLUL or GS), a well-known substrate of $CRL4^{CRBN}$, were unaffected, suggesting that overproduction of GIG WT and mutants did not alter the UPS in *GAN*-KO cells (Fig. 4*F*). Furthermore, NEFM protein levels remained unchanged in all cell lines (Fig. 4 *F–H* and *SI Appendix*, Fig. S13 *A–C*), further confirming that NEFM was not an endogenous substrate of $CRL3^{GIG}$. Taken together, our results indicated that $CRL3^{GIG}$ selectively and specifically targets NF proteins NEFL and INA for degradation by the proteasome and that mutations of GIG at amino acid residues L^{309} and C^{570} fail to interact with and degrade NEFL and INA. These findings may also translate to clinical relevance and account for the mechanisms of pathogenesis underlying GIG mutations in GAN patients, at least in part, at amino acid residues in the Kelch domain.

Mapping the Binding Site of GIG on NEFL. To map the binding site of GIG on NEFL, we generated a series of deletion mutants with the C-terminal MYC tag ($NEFL^{MYC}$). We found that deleting amino acids 237-279 (D4 mutant), including linker L12, coil 2A

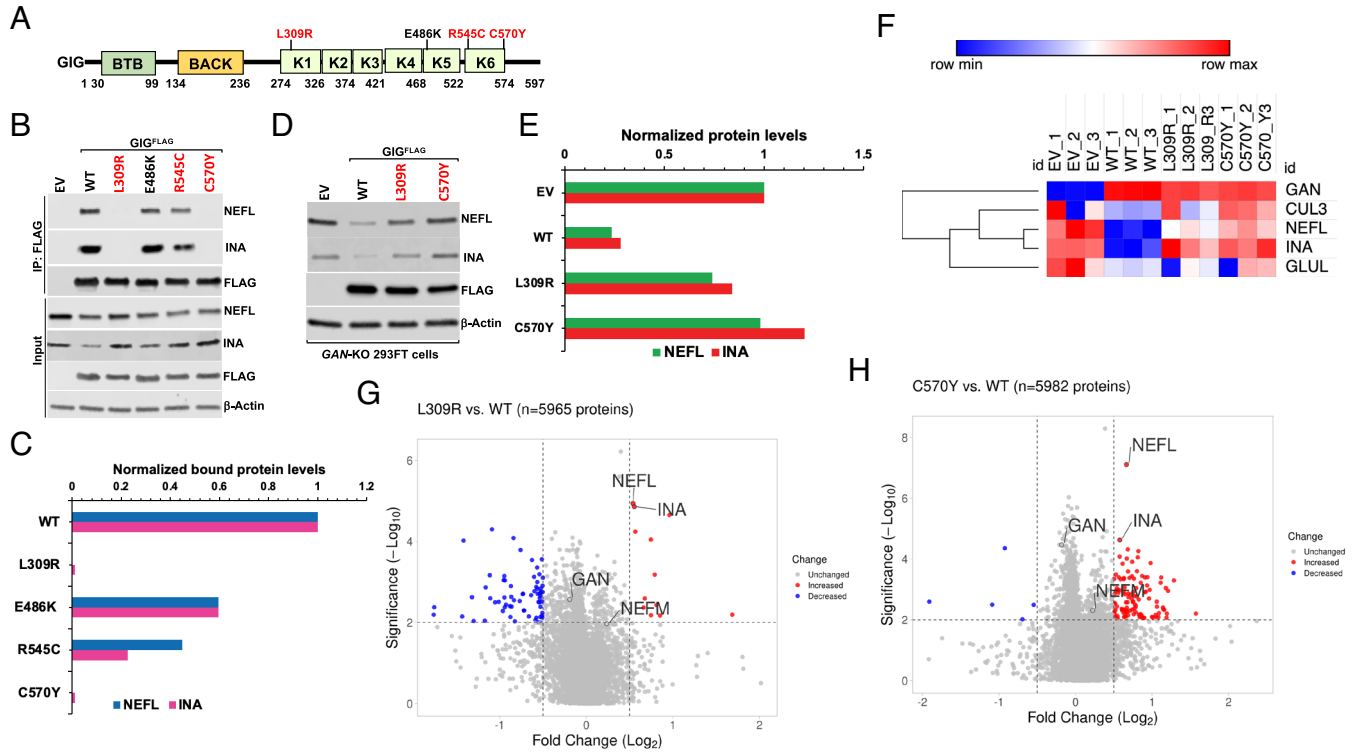

Fig. 4. Mutations in GAN patients at amino acid residues L^{309}, R^{545}, and C^{570} in the Kelch domain of GIG exhibit a loss-of-function mechanism. (*A*) Schematic diagram of human GIG. GIG contains BTB, BACK, and Kelch (K1-6) domains. Highly conserved residues in the Kelch domain of GIG across species, which are mutated in GAN patients, including (L^{309}, R^{545}, and C^{570}), are highlighted in red. (*B*) WT 293FT cells were transfected with empty vector (EV) or wild-type (WT) GIG^{FLAG} and its mutants. After 24 h, cells were treated with 2 μM MLN4924 for 4 h. Cell extracts were immunoprecipitated with anti-FLAG antibody, followed by IB with the indicated antibodies. (*C*) Quantification of NEFL and INA proteins from (*B*). The relative ratios of endogenous NEFL and INA interacted with GIG^{FLAG} to input NEFL and INA, normalized to that of WT in lane 2, are shown. (*D*) Destabilizing endogenous NEFL and INA protein levels in *GAN*-KO cells by WT GIG, but not its mutants. *GAN*-KO16 293FT cells were transfected with EV or WT GIG^{FLAG} and its mutants. After 48 h, cell extracts were analyzed by IB with the indicated antibodies. (*E*) Quantification of NEFL and INA proteins from (*D*). At least three experimental replicates were repeated to optimize conditions (*B* and *D*). (*F–H*) Global proteome analyses (n = 3) of EV-, WT GIG^{FLAG}-, L309R mutant-, and C570Y mutant-transfected *GAN*-KO 293FT cells. The threshold of fold changes was set to more than 1.41-fold increase or decrease and the $-Log_{10}$ P-value above 2. The data were depicted as a heatmap (*F*) and volcano plots for L309R vs. WT (*G*), and C570Y vs. WT (*H*). The red and blue dots denote significantly enriched or reduced proteins, respectively.

subdomain, and linker L2, abolished the binding to GIG (Fig. 5 *A* and *B*). We reconfirmed the D4 mutant using untagged NEFL WT and mutants with antibodies against the N- or C-terminal epitopes on NEFL (*SI Appendix*, Fig. S14 *A* and *B*). To identify the minimal sequence on NEFL required for binding to GIG, we designed biotinylated synthetic L12, 2A, and L2 peptides (Fig. 5*C*) and performed the peptide pulldown assays. As shown in Fig. 5*D*, the NEFL^{L12} peptide, but not NEFL^{2A} and NEFL^{L2} peptides interacted with the ^{GST}GIG protein in vitro. The dot blot analysis also confirmed that ^{GST}GIG bound to NEFL^{L12} peptides but not NEFL^{2A} and NEFL^{L2} peptides (*SI Appendix*, Fig. S15*A*). Intriguingly, the sequence alignment analysis uncovered that the L12 region was highly conserved from zebrafish to humans in both NEFL and INA orthologs (*SI Appendix*, Fig. S16), but it was significantly diversified from the L12 regions of NEFM and NEFH (Fig. 5*A*). This likely stems from evolution and diverse natural selection pressures that allows individual NF subunit to have multiple layers of regulation and functions in neurons. We hypothesized that the NEFL^{L12} segment contains a specific degradation signal for GIG, which does not exist in the L12 regions of NEFM and NEFH proteins. To test this idea, we generated a biotinylated synthetic NEFM^{L12} peptide (M-L12) (Fig. 5*C*) and compared its binding to GIG with the NEFL^{L2} peptide. The peptide pulldown and dot blot analyses revealed that the NEFM^{L12} peptide was not recognized by GIG (Fig. 5*E* and *SI Appendix*, Fig. S15*B*). Collectively, these findings suggested that the L12 segment of NEFL is required for the GIG-NEFL interaction.

Identification of Molecular Basis for the Specific Recognition of NEFL by GIG. We further analyzed the sequence alignment to identify the molecular basis for the GIG-NEFL interaction. We found that the ExD/E motif on NEFL and INA is evolutionarily conserved (Fig. 6*A*). Interestingly, NEFL-D248 is replaced by K and R on NEFM and NEFH, respectively. We reasoned that the core NEFL^{L12} degron was (QISV**E**M**D**V) (Fig. 6*A*), which was required for its binding, ubiquitylation, and degradation. To test this hypothesis, we first performed modeling and in silico study of the NEFL^{L12} degron binding to GIG. The amino acid sequence of GIG (Uniprot ID: Q9H2C0) was used to build a model of the protein's 3D structure using Alphafold2 (41). The NEFL^{L12} degron was observed to bind to the 6-bladed β-propeller KELCH domain of GIG, and its three residues EMD are in direct contact with C570 (Fig. 6 *B* and *C* and *SI Appendix*, Table S2). The binding site of the NEFL^{L12} degron is also located closely to L309 and R545 (Fig. 6*B*). Van der Waals interactions play an essential role in stabilizing the NEFL^{L12} degron in the binding pocket in comparison to hydrogen bonds and hydrophobic interactions. When docked to WT GIG, the NEFL^{L12} degron had a good docking score (*SI Appendix*, Table S2*B*). Consistent with the notion that mutations of the *GAN* gene in GAN patients exhibit the loss-of-function mechanism (Fig. 4 *B*–*E*), a docking score of the C570Y mutant was much higher (*SI Appendix*, Table S2*B*), indicating that this mutation affected the binding of GIG to the NEFL^{L12} degron. The change in binding energy was mainly observed in Van der Waals interactions (*SI Appendix*, Table S2*B*). To validate our computational data, we mutated the motif **EMD** into **AMA** called 2A mutant and found that the binding of 2A mutant to GIG was reduced (Fig. 6 *D* and *E*). Remarkably, the 2A mutant was not ubiquitylated, which substantially suppressed its degradation in cells (Fig. 6 *F*–*H*).

Discussion

In this study, we find that the CRL3^{GIG}–USP15 pathway governs the destruction of NF proteins NEFL and INA, as illustrated in Fig. 7. Surprisingly, CRL3^{GIG} also regulates the stability of actin filament–associated regulatory proteins, including TPM1, TPM2, TAGLN, and CNN2 via direct ubiquitylation. This may account for mutations in GAN patients, characterized by abnormal accumulation of intermediate filaments in neuronal and non-neuronal cells. CRL3^{GIG} may regulate a vast repertoire of substrates and plays an essential role in regulating both NF filaments and actin filaments (via their regulatory protein). Intriguingly, the present work and a recent study (28) demonstrate the biological significance of USP15

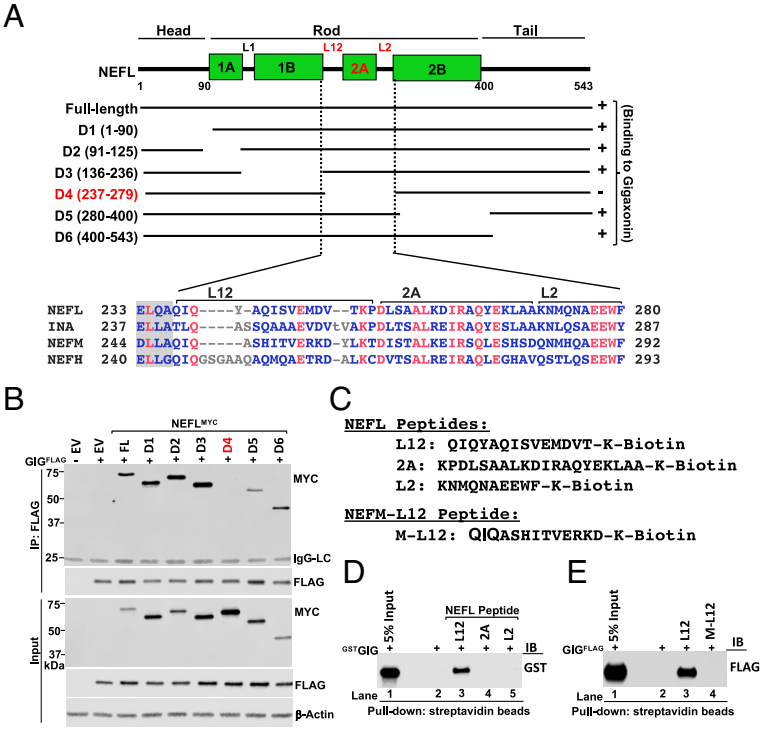

Fig. 5. Mapping the binding site of GIG on NEFL. (*A*) Schematic diagram of human NEFL protein. NEFL includes head, rod, and tail domains. The rod domain contains coil 1A, 1B, 2A, and 2B subdomains, separated by linkers L1, L12, and L2. Deletion of amino acids 237–279 (D4) highlighted in red abolished the binding to GIG, indicating that this sequence contains the NEFL degron recognized by GIG. The sequence alignment of L12, 2A, and L2 segments from human NEFL, INA, NEFM, and NEFH was shown. (*B*) 293FT cells were transfected with the indicated plasmids expressing GIG^{FLAG} and full-length (FL) or deletions of NEFL^{MYC} for 40 h. Cellular extracts were immunoprecipitated with anti-Flag antibody, followed by IB with antibodies against MYC and FLAG. A band ~ 25 kDa (top panel) represents IgG light chains (IgG-LC). (*C*) Design of NEFL-L12, -2A, -L2 and NEFM-L12 (M-L12) peptides. (*D*) Peptide pull-down assays were performed using ^{GST}GIG protein and NEFL-L12, -2A, and –L2 peptides (lane 2 without peptide used as negative control), followed by analyzed by IB with anti-GST antibody. (*E*) Same as (*D*), except that GIG^{FLAG} protein and NEFM-L12 (M-L12) were used. Data are representative of three independent experiments (*B*, *D*, and *E*).

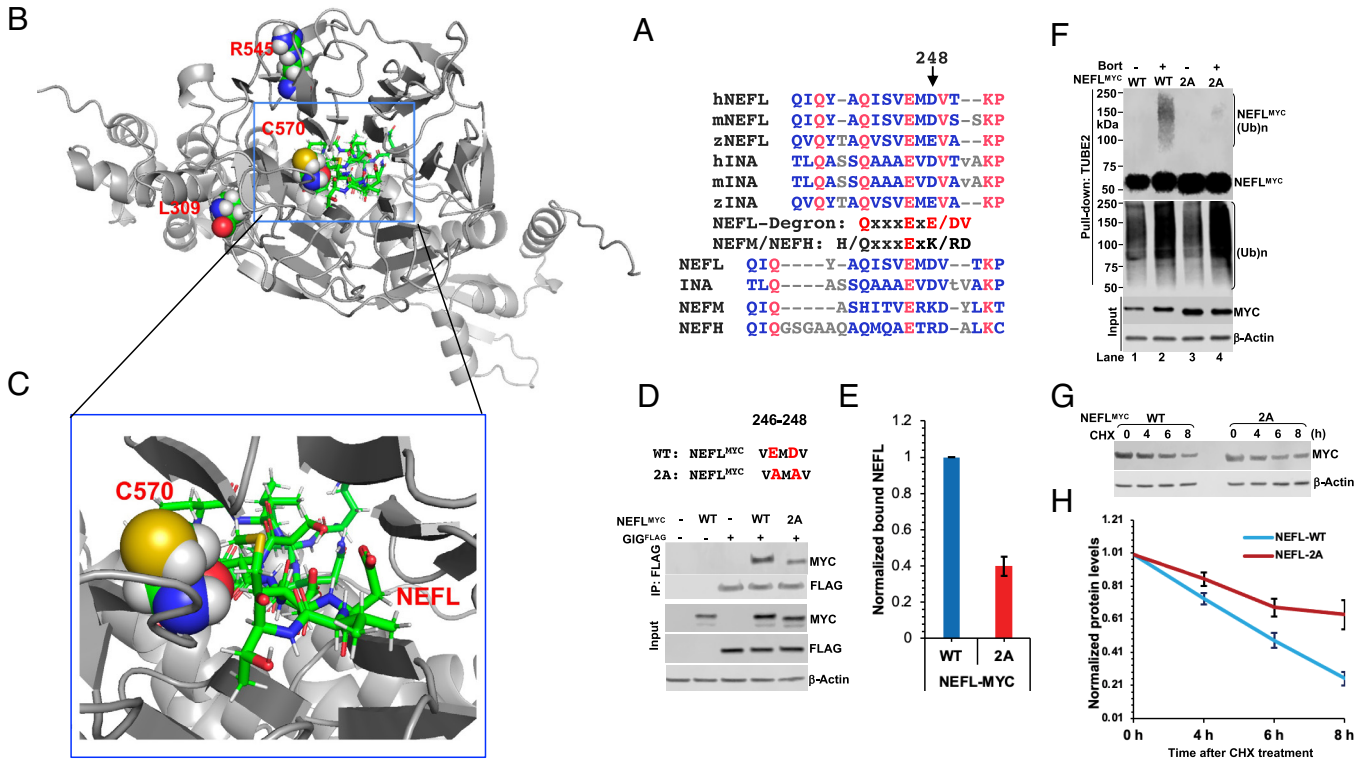

Fig. 6. Identification of molecular basis for the specific recognition of NEFL by GIG. (*A*) L12 segments from human (h), mouse (m), and zebrafish (z) NEFL and INA orthologs and from human NEFL, INA, NEFM, and NEFH. (*B*) Docking pose of the NEFL^{L12} degron to GIG (n = 10). The NEFL^{L12} degron binds to the Kelch domain of GIG and directly interacts with residue C570 located close to residues L309 and R545. (*C*) A close view of electrostatic interactions between residue C570 and the motif ExD. (*D*) WT 293FT cells, transfected with the indicated plasmids expressing GIG^{FLAG} and NEFL^{MYC} WT or 2A mutant for 24 h, were treated with 2 μM MLN4924 for 4 h. Cell extracts were immunoprecipitated with anti-Flag antibody, followed by IB with antibodies against MYC and FLAG. (*E*) Quantification of NEFL^{MYC} protein interacted with GIG^{FLAG} from (*D*). Error bars represent ±SD; n = 2. (*F*) 293FT cells, transfected with NEFL^{MYC} WT or 2A mutant for 40 h, were treated with bortezomib (Bort, 2 μM) for 7 h. Total ubiquitylated proteins were purified using TUBE2-agarose, followed by IB with anti-MYC and anti-ubiquitin antibodies. (Ub)n, polyubiquitin. (*G*) Same as (*F*), except that cells were treated with CHX at the indicated times. Cell extracts were analyzed by IB with anti-MYC and Actin. (*H*) Quantification of NEFL-MYC protein from (*G*). Error bars represent ±SD; n = 2.

in regulating CRL activity. USP15 antagonizes the CRL3^{GIG}-dependent ubiquitylation of NEFL and INA and the CRL4^{CRBN}-mediated ubiquitylation of GS and neosubstrates (28). However, many fundamental questions in future research need to be addressed. For example, NFs are intermediate filaments with a diameter of 10 nm heteropolymers and micrometers in length, which extensively interact with a cytoskeletal protein network of exceptional stability (half-life of many months) and provide structural support to maintain the large calibers of myelinated axons crucial for nerve conduction velocity (18). In mature neurons, NF proteins exist mainly in stable polymers, while the pool of soluble NF proteins is small (42). How does the CRL3^{GIG}-USP15 pathway maintain proper NF protein homeostasis under physiological and stress conditions? Does ubiquitylation of NEFL and INA proteins occur as monomer or

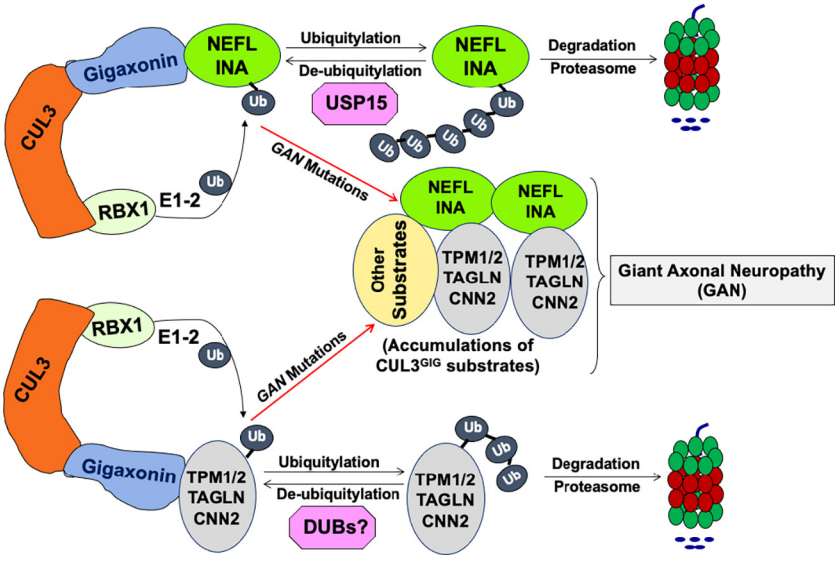

Fig. 7. Proposed model: the CRL3^{GIG}–USP15 pathway governs the destruction of neurofilament proteins NEFL and INA. CRL3^{GIG} also regulates the ubiquitylation of actin filament–associated regulatory proteins (TPM1, TPM2, TAGLN, and CNN2), which DUBs may deubiquitylate. Mutations in the *GAN* gene encoding Gigaxonin cause giant axonal neuropathy (GAN), characterized by abnormal accumulation of intermediate filaments in both neuronal and non-neuronal cells. Thus, CRL3^{GIG} may regulate a vast repertoire of substrates. For the sake of simplicity, the homodimerization of Gigaxonin is omitted.

heteropolymers and require other signals or cofactors? If NEFL and INA subunits are ubiquitylated by $CRL3^{GIG}$ in heteropolymers, whether the extraction of ubiquitylated NF subunits from heteropolymers requires VCP/p97 (43) or new factors so that they can be degraded by the proteasome (44, 45). Moreover, it remains to be elucidated whether USP15 or other DUB may control the turnover of actin filament–associated regulatory proteins.

Actin filament–associated regulatory proteins TPM1, TPM2, TAGLN, and CNN2 are essential in many cellular pathways. Our findings that $CRL3^{GIG}$ directly ubiquitylates TPM1, TAGLN, and CNN2 in vitro and promotes their turnover in cells suggest that $CRL3^{GIG}$ regulates actin filaments. TPM1 mutations in humans cause hypertrophic cardiomyopathy (46, 47). The tension-dependent degradation of CNN2 plays a critical role in regulating the stability of lung alveolar cytoskeleton with physiological and pathological significances via an unknown mechanism (48). In addition, CNN2 was found in a lysophagy proteome landscape study (49), suggesting that it may regulate the lysophagy pathway. Consistent with this idea, a recent study by Kravic et al. demonstrated that the unknown E3-dependent ubiquitylation of CNN2 and the Arp2/3 complex translocate to damaged lysosomes and regulate actin filaments to drive phagophore formation for efficient lysophagy in a p97-dependent manner (50). Future work is needed to dissect the role of $CRL3^{GIG}$-mediated ubiquitylation of actin filament–associated regulatory proteins in various biological processes under physiological and pathological conditions.

Abnormal accumulations of cytoskeleton proteins are neuropathological hallmarks of many neurodegenerative diseases, including Alzheimer's disease, Parkinson's disease, and amyotrophic lateral sclerosis, characterized by filamentous aggregates of NF proteins or intracellular inclusions of aggregated tau proteins (18, 51). Moreover, genetic mutations in genes encoding for IF proteins account for more than 80 diseases (15). For example, mutations in the *NEFL* gene affect the NF network, thus leading to the Charcot–Marie–Tooth disease (52, 53). Another question of interest is whether the dysfunction of the newly discovered $CRL3^{GIG}$–USP15 pathway may contribute to the pathogenesis of these neurodegenerative diseases.

An interesting question is whether the degrons found in another subset of $CRL3^{GIG}$ substrates (TPM1, TAGLN, and CNN2) are similar to the $NEFL^{L12}$ degron. We could not exclude the possibility that these degrons may not have the same motifs because E3 ligases usually regulate multiple substrates and have numerous biological functions under various physiological conditions. For example, the degrons identified among endogenous substrates of $CRL4^{CRBN}$, such as MEIS2, GS, and AMPK gamma are very distinct (54–56). Future work focused on identifying the molecular basis for the NEFLL12 degron-GIG interaction requires a crystal structure of the degron bound to a C-terminal Kelch domain of GIG or a cryo-EM structure of the $CUL3^{GIG}$-NEFL complex. This information is critical for developing molecular glue and PROTAC degraders based on $CRL3^{GIG}$ E3 ligase to treat neurodegenerative disorders.

Materials and Methods

Generation of *GAN*-knockout 293FT Cells by CRISPR/Cas9 Genome Editing. *USP15*-KO 293FT cells were described in our recent protocol (28). This protocol was used for generating *GAN*-KO 293FT cells (28). Briefly, 293FT cells, cultured in a 24-well plate, were transiently transfected with 0.5 μg of human *GAN* CRISPR/Cas9 plasmids using Fugene HD. Two days after transfection, a single cell was seeded in a 96-well plate via serial dilutions. After 10–12 d, single clones were obtained, cultured in 24-well plates, and expanded for 5–7 d to validate the editing of *GAN* by western blot.

RNA-Sequencing Analysis. RNA-sequencing (seg) was done using RNAs isolated from wild-type (WT), *USP15*-KO, MLN4924-treated *USP15*-KO, and *GAN*-KO 293FT cells as described in *SI Appendix*.

Proteomic Analysis. The detailed protocols for proteomic analyses of WT, *USP15*-KO, and *GAN*-KO 293FT cell lines were described in *SI Appendix*.

In Vitro Ubiquitylation, Deubiquitylation, and Competitive Ubiquitylation/Deubiquitylation Assays. The in vitro ubiquitylation assays were performed as described previously (28, 56). Briefly, the assays were carried out for 1 h at 30 °C in a final volume of 30 μL containing 200 ng of substrates (rNEFL, rINA, rTPM1, rCNN2, or rTAGLN), E1, E2 (UbcH5a and UbcH3/Cdc34), $CLR3^{GIG}$ complex (200 ng NEDDylated RBX1-CUL3, mixed with 200 ng ^{GST}GIG), and ^{HA}Ub (HA-tagged wild-type ubiquitin). The in vitro deubiquitylation assays using rUSP15 (1 μg) were performed as described previously (28, 43). The in vitro competitive ubiquitylation/deubiquitylation assays were described in a recent study (28).

Peptide Pull-Down and Dot Blot Assays. The detailed peptide pull-down and dot blot assays were described in *SI Appendix*.

Data, Materials, and Software Availability. All study data are included in the article and/or supporting information.

ACKNOWLEDGMENTS. We would like to thank LC Sciences (Houston, TX) for assisting with RNA-sequencing experiments. This research was in part supported by the Memorial Sloan Kettering Cancer Center Support Grant P30CA008748 (A.O.), the Basic Science Research Program through the National Research Foundation of Korea funded by the Ministry of Education (2021R1A6A3A14038416) to K.H.N., the Nano Material Technology Development Program (No. 2016M3A7B6908929) of NRF funded by the Ministry of Science and ICT (J.E.L.), institutional fund by the University of Missouri-Columbia (T.V.N.), and the National Institute of General Medical Sciences of the NIH Grant R01GM148470 (T.V.N.).

Author affiliations: [a]Biometrology Group, Korea Research Institute of Standards and Science, Daejeon 34113, Korea; [b]Division of Quantum Simulation and Optimization, SandboxAQ, New York, NY 10591; [c]Gehrke Proteomics Center, Christopher S. Bond Life Sciences Center, University of Missouri, Columbia, MO 65211; [d]Cell Biology Program, Sloan Kettering Institute, Memorial Sloan Kettering Cancer Center, New York, NY 10065; and [e]Center for Precision Medicine, Department of Medicine, University of Missouri, Columbia, MO 65212

1. A. Varshavsky, The ubiquitin system, an immense realm. *Annu. Rev. Biochem.* **81**, 167–176 (2012).
2. A. Hershko, A. Ciechanover, The ubiquitin system. *Annu. Rev. Biochem.* **67**, 425–479 (1998).
3. X. Huang, V. M. Dixit, Drugging the undruggables: Exploring the ubiquitin system for drug development. *Cell Res.* **26**, 484–498 (2016).
4. M. D. Petroski, R. J. Deshaies, Function and regulation of cullin-RING ubiquitin ligases. *Nat. Rev. Mol. Cell Biol.* **6**, 9–20 (2005).
5. J. W. Harper, B. A. Schulman, Cullin-RING ubiquitin ligase regulatory circuits: A quarter century beyond the F-Box hypothesis. *Annu. Rev. Biochem.* **90**, 403–429 (2021).
6. S. Duan, M. Pagano, Ubiquitin ligases in cancer: Functions and clinical potentials. *Cell Chem. Biol.* **28**, 918–933 (2021).
7. P. J. Stogios, G. S. Downs, J. J. Jauhal, S. K. Nandra, G. G. Prive, Sequence and structural analysis of BTB domain proteins. *Genome Biol.* **6**, R82 (2005).
8. M. Furukawa, Y. J. He, C. Borchers, Y. Xiong, Targeting of protein ubiquitination by BTB-Cullin 3-Roc1 ubiquitin ligases. *Nat. Cell Biol.* **5**, 1001–1007 (2003).
9. L. Pintard *et al.*, The BTB protein MEL-26 is a substrate-specific adaptor of the CUL-3 ubiquitin-ligase. *Nature* **425**, 311–316 (2003).
10. L. Xu *et al.*, BTB proteins are substrate-specific adaptors in an SCF-like modular ubiquitin ligase containing CUL-3. *Nature* **425**, 316–321 (2003).
11. D. D. Zhang, S. C. Lo, J. V. Cross, D. J. Templeton, M. Hannink, Keap1 is a redox-regulated substrate adaptor protein for a Cul3-dependent ubiquitin ligase complex. *Mol. Cell Biol.* **24**, 10941–10953 (2004).
12. M. Zhuang *et al.*, Structures of SPOP-substrate complexes: Insights into molecular architectures of BTB-Cul3 ubiquitin ligases. *Mol. Cell* **36**, 39–50 (2009).
13. P. Canning *et al.*, Structural basis for Cul3 protein assembly with the BTB-Kelch family of E3 ubiquitin ligases. *J. Biol. Chem.* **288**, 7803–7814 (2013).
14. A. X. Ji, G. G. Prive, Crystal structure of KLHL3 in complex with Cullin3. *PLoS ONE* **8**, e60445 (2013).
15. M. B. Omary, "IF-pathies": A broad spectrum of intermediate filament-associated diseases. *J. Clin. Invest.* **119**, 1756–1762 (2009).

16. D. Guerette, P. A. Khan, P. E. Savard, M. Vincent, Molecular evolution of type VI intermediate filament proteins. *BMC Evol. Biol.* **7**, 164 (2007).
17. A. Yuan, M. V. Rao, Veeranna, R. A. Nixon, Neurofilaments at a glance. *J. Cell Sci.* **125**, 3257–3263 (2012).
18. A. Yuan, R. A. Nixon, Posttranscriptional regulation of neurofilament proteins and tau in health and disease. *Brain Res. Bull.* **192**, 115–127 (2023).
19. A. K. Asbury, M. K. Gale, S. C. Cox, J. R. Baringer, B. O. Berg, Giant axonal neuropathy–A unique case with segmental neurofilamentous masses. *Acta Neuropathol.* **20**, 237–247 (1972).
20. B. O. Berg, S. H. Rosenberg, A. K. Asbury, Giant axonal neuropathy. *Pediatrics* **49**, 894–899 (1972).
21. R. Tandan *et al.*, Childhood giant axonal neuropathy. Case report and review of the literature. *J. Neurol. Sci.* **82**, 205–228 (1987).
22. C. Bruno *et al.*, Clinical and molecular findings in patients with giant axonal neuropathy (GAN). *Neurology* **62**, 13–16 (2004).
23. P. Opal, "GAN-related neurodegeneration" in *GeneReviews®*, M. P. Adam *et al.*, Eds. (GeneReviews®, Seattle, WA, 1993).
24. P. Bomont *et al.*, The gene encoding gigaxonin, a new member of the cytoskeletal BTB/kelch repeat family, is mutated in giant axonal neuropathy. *Nat. Genet.* **26**, 370–374 (2000).
25. D. Chirnomas, K. R. Hornberger, C. M. Crews, Protein degraders enter the clinic–A new approach to cancer therapy. *Nat. Rev. Clin. Oncol.* **20**, 265–278 (2023).
26. A. D. Cowan, A. Ciulli, Driving E3 ligase substrate specificity for targeted protein degradation: Lessons from nature and the laboratory. *Annu. Rev. Biochem.* **91**, 295–319 (2022).
27. K. M. Sakamoto *et al.*, Protacs: Chimeric molecules that target proteins to the Skp1-Cullin-F box complex for ubiquitination and degradation. *Proc. Natl. Acad. Sci. U.S.A.* **98**, 8554–8559 (2001).
28. T. V. Nguyen, USP15 antagonizes CRL4(CRBN)-mediated ubiquitylation of glutamine synthetase and neosubstrates. *Proc. Natl. Acad. Sci. U.S.A.* **118**, e2111391118 (2021).
29. G. Shaw, S. Morse, M. Ararat, F. L. Graham, Preferential transformation of human neuronal cells by human adenoviruses and the origin of HEK 293 cells. *FASEB J.* **16**, 869–871 (2002).
30. T. T. M. Vu, D. C. Mitchell, S. P. Gygi, A. Varshavsky, The Arg/N-degron pathway targets transcription factors and regulates specific genes. *Proc. Natl. Acad. Sci. U.S.A.* **117**, 31094–31104 (2020).
31. B. L. Johnson-Kerner, A. Garcia Diaz, S. Ekins, H. Wichterle, Kelch domain of gigaxonin interacts with intermediate filament proteins affected in giant axonal neuropathy. *PLoS ONE* **10**, e0140157 (2015).
32. T. A. Soucy *et al.*, An inhibitor of NEDD8-activating enzyme as a new approach to treat cancer. *Nature* **458**, 732–736 (2009).
33. A. L. Goldberg, Development of proteasome inhibitors as research tools and cancer drugs. *J. Cell Biol.* **199**, 583–588 (2012).
34. M. J. Emanuele *et al.*, Global identification of modular cullin–RING ligase substrates. *Cell* **147**, 459–474 (2011).
35. V. Ionasescu *et al.*, Giant axonal neuropathy: Normal protein composition of neurofilaments. *J. Neurol. Neurosurg. Psychiatry* **46**, 551–554 (1983).
36. B. L. Johnson-Kerner *et al.*, Intermediate filament protein accumulation in motor neurons derived from giant axonal neuropathy iPSCs rescued by restoration of gigaxonin. *Hum. Mol. Genet.* **24**, 1420–1431 (2015).
37. F. Dequen, P. Bomont, G. Gowing, D. W. Cleveland, J. P. Julien, Modest loss of peripheral axons, muscle atrophy and formation of brain inclusions in mice with targeted deletion of gigaxonin exon 1. *J. Neurochem.* **107**, 253–264 (2008).
38. T. Ganay, A. Boizot, R. Burrer, J. P. Chauvin, P. Bomont, Sensory-motor deficits and neurofilament disorganization in gigaxonin-null mice. *Mol. Neurodegener.* **6**, 25 (2011).
39. M. Balastik *et al.*, Deficiency in ubiquitin ligase TRIM2 causes accumulation of neurofilament light chain and neurodegeneration. *Proc. Natl. Acad. Sci. U.S.A.* **105**, 12016–12021 (2008).
40. S. Mahammad *et al.*, Giant axonal neuropathy-associated gigaxonin mutations impair intermediate filament protein degradation. *J. Clin. Invest.* **123**, 1964–1975 (2013).
41. J. Jumper *et al.*, Highly accurate protein structure prediction with AlphaFold. *Nature* **596**, 583–589 (2021).
42. A. Yuan, R. A. Nixon, Neurofilament proteins as biomarkers to monitor neurological diseases and the efficacy of therapies. *Front. Neurosci.* **15**, 689938 (2021).
43. T. V. Nguyen *et al.*, p97/VCP promotes degradation of CRBN substrate glutamine synthetase and neosubstrates. *Proc. Natl. Acad. Sci. U.S.A.* **114**, 3565–3571 (2017).
44. D. M. Rubin, D. Finley, Proteolysis., The proteasome: A protein-degrading organelle? *Curr. Biol.* **5**, 854–858 (1995).
45. J. Lowe *et al.*, Crystal structure of the 20S proteasome from the archaeon *T. acidophilum* at 3.4 A resolution. *Science* **268**, 533–539 (1995).
46. A. Karibe *et al.*, Hypertrophic cardiomyopathy caused by a novel alpha-tropomyosin mutation (V95A) is associated with mild cardiac phenotype, abnormal calcium binding to troponin, abnormal myosin cycling, and poor prognosis. *Circulation* **103**, 65–71 (2001).
47. S. J. Carlus *et al.*, A novel homozygous TPM1 mutation in familial pediatric hypertrophic cardiomyopathy and in silico screening of potential targeting drugs. *Eur. Rev. Med. Pharmacol. Sci.* **24**, 7732–7744 (2020).
48. N. Wang, D. E. Ingber, Control of cytoskeletal mechanics by extracellular matrix, cell shape, and mechanical tension. *Biophys. J.* **66**, 2181–2189 (1994).
49. V. V. Eapen, S. Swarup, M. J. Hoyer, J. A. Paulo, J. W. Harper, Quantitative proteomics reveals the selectivity of ubiquitin-binding autophagy receptors in the turnover of damaged lysosomes by lysophagy. *eLife* **10**, e72328 (2021).
50. B. Kravic *et al.*, Ubiquitin profiling of lysophagy identifies actin stabilizer CNN2 as a target of VCP/p97 and uncovers a link to HSPB1. *Mol. Cell* **82**, 2633–2649.e2637 (2022).
51. N. J. Cairns, V. M. Lee, J. Q. Trojanowski, The cytoskeleton in neurodegenerative diseases. *J. Pathol.* **204**, 438–449 (2004).
52. A. M. Rossor, J. M. Polke, H. Houlden, M. M. Reilly, Clinical implications of genetic advances in Charcot-Marie-Tooth disease. *Nat. Rev. Neurol.* **9**, 562–571 (2013).
53. H. J. Kim *et al.*, Phenotypic heterogeneity in patients with NEFL-related Charcot-Marie-Tooth disease. *Mol. Genet. Genomic Med.* **10**, e1870 (2022).
54. S. J. Yang *et al.*, Ubiquitin-dependent proteasomal degradation of AMPK gamma subunit by Cereblon inhibits AMPK activity. *Biochim. Biophys. Acta Mol. Cell Res.* **1867**, 118729 (2020).
55. E. S. Fischer *et al.*, Structure of the DDB1-CRBN E3 ubiquitin ligase in complex with thalidomide. *Nature* **512**, 49–53 (2014).
56. T. V. Nguyen *et al.*, Glutamine triggers acetylation-dependent degradation of glutamine synthetase via the thalidomide receptor cereblon. *Mol. Cell* **61**, 809–820 (2016).